Satellite in-situ electron density observations of the storm enhanced density and the polar Tongue of Ionization on the noon meridional plane in the F region during the 20 November 2003 magnetic storm

Chin S. Lin[1], Eric K. Sutton[2], Wenbin Wang[3], Guiping Liu[4], Carl J. Henney[5], and David L. Cooke[5]

[1]Lins Institute of Science, Waltham, Massachusetts, USA.

[2]Space Weather Technology, Research, and Education Center, University of Colorado at Boulder, Boulder, Colorado, USA.

[3]High Altitude Observatory, National Center for Atmospheric Research, Boulder, Colorado, USA.

[4]Space Sciences Laboratory, University of California Berkeley, Berkeley, CA, USA.

[5]Space Vehicles Directorate, Air Force Research Laboratory. Albuquerque, New Mexico, USA.

Corresponding author: Chin Lin (cnsnln@gmail.com)

Key Points:

- The first report on satellite in-situ electron density measurements of the storm enhanced density at the noon meridian plane
- The lifecycle of ionospheric storm enhanced densities is mainly controlled by variations of the dayside prompt penetration electric fields
- The key methodologies include a comparison of TIEGCM modeling with satellite in-situ electron density observations and a correlation analysis

Abstract

Ionospheric storm enhanced density (SED) has been extensively investigated using Total Electron Content (TEC) deduced from GPS ground and satellite-borne receivers. However, in-situ electron density measurements have not been reported for SEDs yet. We report in-situ electron density measurements of a SED event and its associated polar tongue of ionization (TOI) at the noon meridian plane measured by the CHAMP polar-orbiting satellite at about 390 *km* altitude during the 20 November 2003 magnetic storm. The measurements provided rare evidence about the SED's life cycle at a fixed magnetic local time. CHAMP detected the SED onset right after the arrival of an interplanetary coronal mass ejection shock front. The SED electron density enhancement extended from the equatorial ionization anomaly to the noon cusp, through which plasmas entered into the polar cap as polar plasma clouds/TOI. For several satellite-ground conjunction passes, CHAMP measured the electron density of plasma clouds comparable to the TOI density measured by the Tromso ISR, establishing that the plasma clouds were related to the TOI. The SED plume in the NH retreated gradually to lower latitudes six hours after the SED onset. We conducted TIEGCM modeling to demonstrate that the SED density enhancement was likely due to the vertical transport of plasmas. The observed mid-latitude electron density varied with the cross-polar cap electric fields, suggesting that prompt penetration electric fields (PPEFs) in the zonal direction played a dominant role. The implication is that variations of the dayside PPEFs largely control the SED lifecycle.

Plain Language Summary

Ground radar and GPS stations have frequently detected enhancement of ionospheric electron density at mid-latitudes and in the polar cap during the magnetic storm recovery phase. We report in-situ satellite observations near 400 *km* at the noon meridian plane during an intense magnetic storm. It provides for the first time clear evidence about the life cycle of ionospheric electron density enhancement, starting from its onset at mid-latitudes, entry into the polar cap, and retreat to lower latitudes. The mid-latitude ionospheric electron density was mainly enhanced in the northern hemisphere, triggered by the passage of a solar wind dynamic pressure shock front. Global circulation modeling suggests that the vertical transport of ionospheric plasmas probably produced the enhancement. The dayside prompt-penetration electric fields in the zonal direction likely drove the vertical plasma uplift. Thus, it appears that the SED lifecycle is mainly controlled by variations of the dayside prompt electric field.

1 Introduction

Ionospheric storm time-enhanced density (SED) and the tongue of ionization (TOI) are prominent ionosphere structures that were first observed at high latitudes and in subauroral regions in the afternoon sector during the recovery phase of geomagnetic storms (e.g., Papagiannis et al., 1971; Mendillo et al., 1972; Evans, 1973; Anderson, 1976; Foster, 1993; Buonsanto, 1995, 1999). Foster (1993) named the SED to characterize the Millstone Hill Incoherent Scatter Radar (ISR) measurements that frequently show dramatic F region electron density enhancements around the duskside. Characteristics of the SED phenomenon typically include a latitudinally distinct region of sunward convection F region plasma, high electron densities, an elevated F region peak, a significantly enhanced topside ionosphere, and low electron temperatures near sunset at middle latitudes (Foster, 1993; J. Liu et al., 2015, 2016).

With the advent of GPS receiver measurements from the global International GNSS Services (IGS) network, SED events have been extensively studied using the remote sensing of ionospheric Total Electron Content (TEC) from GPS ground stations (e.g., Coster and Skone, 2009). These ground GPS receiver data provide detailed global TEC maps that have been used to characterize both temporal and spatial features about the SED (e.g., Correia et a., 2017; Adebiyi et al., 2019; Sori et al., 2019). Similar upward vertical TEC (VTEC) data above the satellite altitudes obtained by GPS receivers onboard the satellites had provided additional insights about the SED dynamics during three major magnetic storms (Mannucci et al., 2008; Mannucci et al., 2014). Their studies suggested that the interplanetary magnetic field (IMF) By component may influence the TEC response during the main phase of superstorms. Verkhoglyadova et al. (2017) revisited these three complex magnetic storms to estimate the efficiency of the solar wind-magnetosphere connection. They found that the overall VTEC maxima are generally delayed by ~2–3 *hr* relative to the maxima of the coupling functions. Yue et al. (2016) assimilated observations from ground- and multiple LEO satellite-based GNSS-observed slant TEC and nadir VTEC from the Jason satellites' altimeters during the 17 March 2013 geomagnetic storm. They showed that the global ionospheric electron density had dynamic and complicated time evolution features, including the polar cap TOIs and auroral boundary blobs.

Reports of satellite in-situ electron density measurements in regions of SED and TOI are rare. Foster et al. (2005) examined ion drift meter measurements of the Defense Meteorological Satellite Program (DMSP) satellite to describe the polar cap convection pattern associated with the SED/TOI. However, they did not report on the in-situ electron density. Horvath and Lovell (2015) used the ground- and space-based TEC observational data to investigate the ionosphere's global response in two SED events during the 15 May 2005 superstorm. They analyzed the multi-instrument in situ measurements of the DMSP satellite to construct various latitudinal profiles of electron density and ion drift velocities related to the SED at around 850 *km*. In essence, in-situ electron density variations of the SED and TOI in the F-region below 600 *km* have not been investigated yet. We present in this paper in-situ electron density measurements by the CHAMP satellite at about 390 *km* related to the SED and TOI, which were observed throughout the 20 November 2003 magnetic storm.

Several studies have previously investigated various aspects of the ionosphere-thermosphere responses observed during the 20 November 2003 storm. The SED and its TOI event observed at high latitudes in the northern hemisphere (NH) during the storm had been studied in detail by Foster et al. (2005). They used high-latitude incoherent scatter radars and DMSP observations of in situ plasma parameters and north polar maps of stormtime plumes of enhanced TEC derived from a network of GPS receivers to examine the TOI circulation pattern. They concluded that the dayside source of the TOI is presumably the SED plume transported from low latitudes in the postnoon sector to the polar cap by the subauroral disturbance electric field. Yizengaw et al. (2006) employed an extensive dataset, including ground GPS receivers, ionosonde, magnetometers, and the GPS receiver onboard CHAMP satellite during the November 2003 storm, to analyze the mid-latitude ionospheric response. They showed that the ionospheric F2-layer peak height had been depressed down to altitudes below 350 *km* before 16 *hr* UT. Mannucci et al. (2008) further examined vertical TEC measurements by the CHAMP GPS receiver along the line of sight from the CHAMP satellite to GPS satellites during this event. They found a delay in low- to middle-latitude daytime upward VTEC increases above the satellite. The VTEC significant enhancement peak appeared for several hours (5–7) after the

IMF B_z component turned southward, much later than the 2-3 hours delay seen in the other magnetic storm events. Notably, the VTEC enhancement reached a peak in an interval of a large interplanetary magnetic cloud passing through the Earth. Verkhoglyadova et al. (2017) later asserted that a strong IMF *By* component might cause the long delay of the afternoon VTEC peak, possibly through modifying the high-latitude convection pattern (Crowley et al., 2010; Mannucci et al., 2014).

We briefly describe solar wind drivers and the *Sym-H* index for the 20 November 2003 magnetic storm in Section 2. Then, section 3 presents CHAMP in-situ plasma observations of the SED and the CHAMP-ISR conjunction observations of the TOI. Next, we compare the TIEGCM modeling with the CHAMP observations in Section 4. We then discuss the SED life cycle and the role of prompt penetration electric fields in Section 5. We also present a correlation analysis of the enhanced density with the estimated cross-polar cap electric fields. Finally, we put forth the conclusions in Section 6.

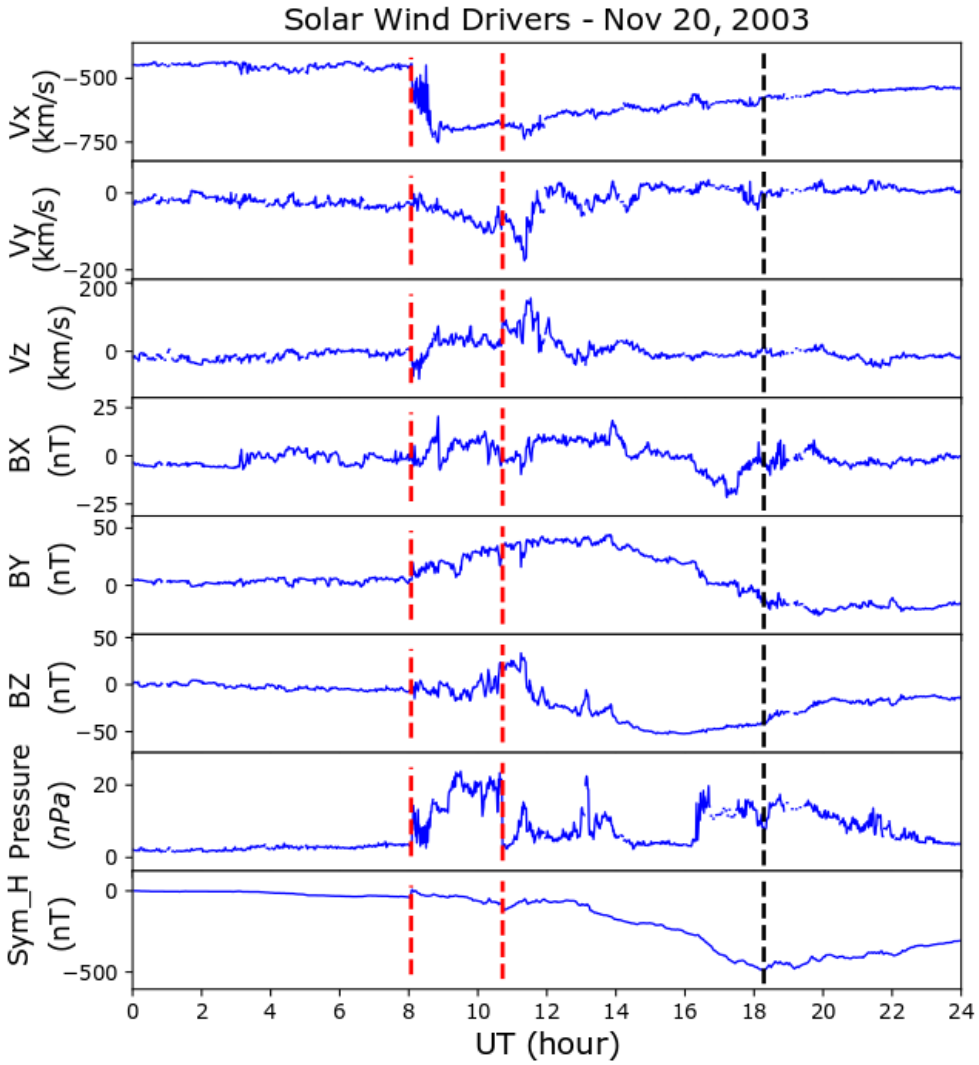

Figure 1. Solar wind parameters at Earth's location and the *Sym-H* index for the 20 November 2003 magnetic storm. Panels from top to bottom are velocity components (*Vx*, *Vy*, and *Vz*), magnetic field components (*Bx*, *By*, and *Bz*), solar wind dynamic plasma pressure in *nPa*, and the *Sym-H* index. The first red dotted line marks the arrival of an interplanetary shock, whereas the second red dotted line marks the appearance of a strong magnetic cloud. The black dotted line marks the peak of the magnetic storm activity.

2 20 November 2003 Magnetic Storm

An interplanetary coronal mass ejection swept by the Earth on 20 November 2003, causing an intense magnetic storm (Echer et al., 2008). Figure 1 displays the solar wind parameters at Earth's location for this event. These parameters provided by the NASA OMNIweb 5-minute dataset (https://omniweb.gsfc.nasa.gov/) have been deduced by time-shifting the solar wind magnetic field and plasma data measured by the ACE satellite to the Earth's bow shock nose. It shows an interplanetary forward shock front about 08:04 UT (marked by the first red dotted line). It passed through Earth's magnetosphere and caused a storm sudden commencement (SSC) with an amplitude of about 42 *nT*. Across the shock front, solar wind density increased from 6 to 20 cm^3, velocity from 440 to 610 *km/s*, solar wind ram pressure from 3 to 8 *nPa*, and IMF intensity (|*B*|) from 8.2 *nT* to 15.4 *nT* (Echer et al. 2008). The solar wind dynamic (ram) pressure had a pulse with an average magnitude of 15 *nPa* (second from the bottom panel). After the shock, the solar wind dynamic pressure continued to increase until 10:43 UT, when the pressure suddenly dropped to a low value around a few *nPa* in response to a magnetic cloud (MC) arrival (second red dotted line). The IMF *Bz* component in the MC was initially predominantly northward and did not produce significant magnetic disturbance (third from bottom panel). Magnetic field rotated from *+Y* to southward direction after 12 *hr* UT, and then *-Y* direction after 20:00 UT. The *Vy* and *Vz* velocity components connected with the *By* rotation had a pulse reaching 200 *km/s* at 11:30 UT (second and third panel, respectively). The magnetic field inside the MC was very intense after 13:00 UT culminating in a peak magnitude of 51 *nT* for the southward *Bz* and producing a severe magnetic storm. The *Sym-H* started to decrease after about 13:00 UT and reached a minimum of about -500 *nT* at 18:17 UT (bottom panel and marked by black dashed line). After 19:00 UT, the storm recovered gradually until the end of the day. See Echer et al. (2008) and Han et al. (2014) for a detailed description.

3 Observations

The CHAMP satellite was circulating in a near-polar orbit (inclination: 87.3°) near the noon magnetic local time (MLT) meridional plane at about 390 *km* during the 20 November 2003 magnetic storm. The plasma density dataset we analyzed contains electron density measurements by the Planar Langmuir Probe (PLP) onboard the CHAMP satellite (Cooke et al., 2003; McNamara et al., 2007). The PLP consisted of a gold 152 x 203 *mm* rectangular plate mounted on the lower front panel of the spacecraft. The sensor plate of the PLP with a normal aligned with the forward axis of the spacecraft is alternately allowed to float for 14 *s* to track the spacecraft potential and sweep in voltage for 1 *s* to verify the floating potential and determine electron density and electron temperature. Thus, the electron density dataset has a time resolution of 15 *s*. Under the condition of quasi-neutrality, the plasma density is the same as electron density. Therefore, we shall consider electron density measured by the PLP to be the same as plasma density. The PLP electron density measurements have been verified with

digisonde recordings by McNamara et al. (2007). They estimated that the average discrepancy between PLP and digisonde recordings is about 4%, with a standard deviation of 8.8%. Several studies have examined this plasma dataset, including solar activity dependence of the electron density in equatorial ionization anomaly (EIA) regions (H. Liu et al., 2007), comparison of ionospheric electron density with the IRI model (Lühr and Xiong, 2010), and simultaneous observations of polar plasma clouds with polar cap neutral density enhancement (Lin et al., 2018).

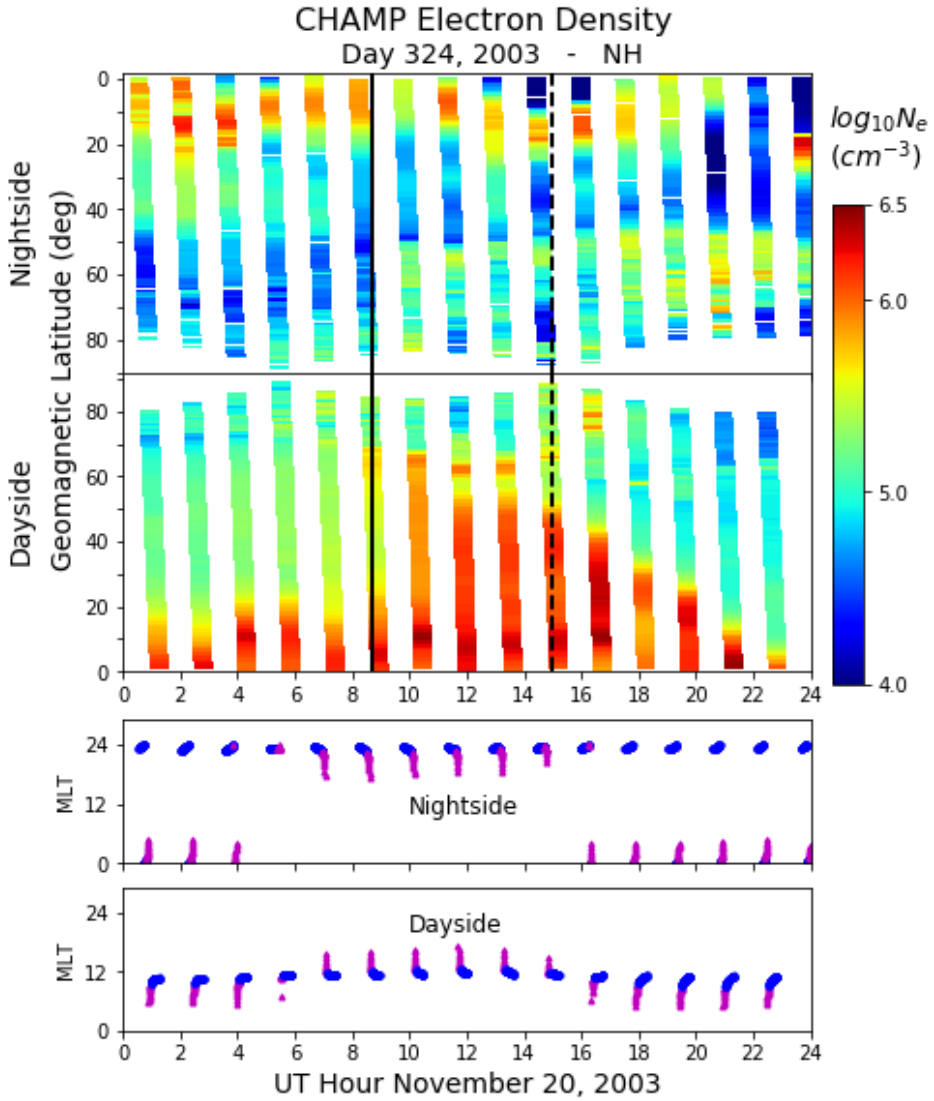

Figure 2. Electron density measured along the CHAMP orbit in the northern hemisphere on 20 November 2003. In the top panel, each color strip from top to bottom shows electron density from the nightside equator (top boundary of the top panel) to the polar cap. Each color strip in the second panel shows electron density from the polar cap to the dayside equator. The ordinate is geomagnetic latitude. The nightside and dayside MLTs are presented in the third and

fourth panels, respectively. Blue dots mark MLT for geomagnetic latitude (Mlat) less than 60^o. In these two MLT panels, traces of MLT in the polar cap appear as magenta hooks.

3.1 Northern hemisphere observations

The electron density measured along the CHAMP orbit in the NH on the noon-midnight meridional plane on 20 November 2003 is shown in Figure 2. Each color strip displays electron density from the nightside equator (top boundary of the top panel) to the polar cap in the top panel and represents density from the polar cap to the dayside equator in the second panel. The color strips have gaps near the polar cap in the magnetic latitude-Universal Time (Mlat-UT) plot because CHAMP often did not reach 90^o MLat. We plot the CHAMP MLT in the third panel for nightside passes and the bottom panel for dayside passes. In the mid-latitude range (Mlat < 60^o), CHAMP MLT was about 12 *hr* on the dayside (blue dots, bottom panel) and about 24 *hr* MLT on the nightside (blue dots, third panel). CHAMP quickly passed through a range of MLT in the polar cap, appearing as magenta hooks in these two panels.

About half an hour after the ICME shock arrival at Earth's magnetopause, CHAMP detected a distinct electron density localized enhancement around 60^o MLat near noon MLT in the NH around 08:40 UT (solid line in Figure 2). Thus, it seemed that the SED first exhibited as a localized density enhancement at high latitudes near noon. CHAMP detected weak electron density enhancement from 20^o to 60^o MLat in this pass as well. In the subsequent CHAMP passes (from 10:00 UT to 18:00 UT), the mid-latitude density increased significantly, about one order of magnitude from low $log_{10}Ne = 5\ cm^{-3}$ before the onset (~ 08:00 UT) to $Log_{10}Ne = 6\ cm^{-3}$ a few hours after the onset. During this interval, the solar wind velocity became stabilized and remained high. As described in Section 2, the IMF B_Z turned southward and continued to increase. It reached a maximum value of 51 *nT*, likely resulting in significant solar wind *E*x*B* electric fields. This timeline indicates that the ICME shock triggered the SED, and the IMF magnetic cloud and large solar wind velocity drove the midlatitude electron density enhancement.

The SED reached the dayside cusp for 5-6 hours from about 08:40 to 15:00 UT (Figure 2, second panel). Then, it started to retreat gradually to lower MLats starting around 15:00 UT (dashed line), and the retreat continued till the end of the day. Its high MLat boundary decreased from about 50^o Mlat at 14 *hr* UT linearly to the equator at 23 *hr* UT.

Champ satellite detected patches of electron density enhancements inside the polar cap (MLat > 65^o) in tandem with the SED onset. The polar cap density was patchy between 60^o and 80^o MLat on the nightside (top panel, Figure 2). Therefore, the CHAMP in-situ observations have suggested that the SED plasma had entered through the dayside cusp and observed as polar plasma clouds or TOI. These TOI plasma clouds were moving from dayside to nightside on the noon-midnight meridional plane. The polar cap electron density enhancement exhibited a low MLat cutoff around 50^o Mlat on the nightside (top panel). This cutoff means that the polar TOI did not drift to lower than the auroral zone Mlat. The plasma clouds were probably following convection streamlines before reaching the auroral oval boundary.

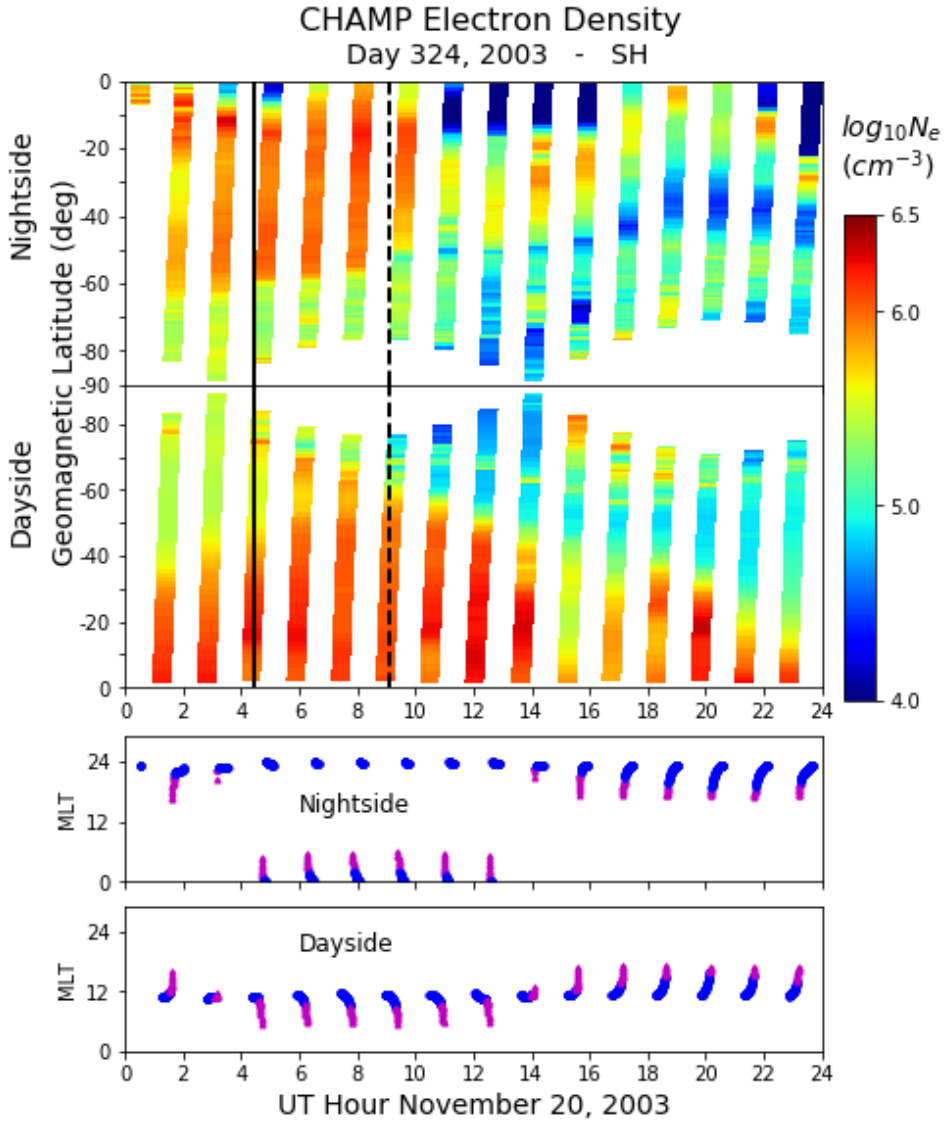

Figure 3. Electron density measured along the CHAMP orbit in the southern hemisphere on 20 November 2003 in the same format as Figure 2. A solid line around 04:25 UT marks the beginning of the SH precursory density enhancement. The retreat of the SH precursory density enhancement begins at 09:05 UT, marked by a dashed line.

3.2 Southern hemisphere observations

The CHAMP electron density observations have indicated interesting hemispheric asymmetry. Figure 3 presents electron density measured by CHAMP in the southern hemisphere (SH) in the same format as Figure 2. CHAMP detected SH dayside electron density enhancement about 04:25 UT (marked by a solid line in Figure 3) more than three hours before the ICME shock arrival and the SED onset. This SH precursory density enhancement seemed

to be unrelated to magnetic disturbances since *Sym-H* was quiet and steady. It withdrew to lower MLat after 09:05 UT (marked by a dashed line) when the SED was building up in the NH. The reason for these unexpected features in the summer hemisphere is unclear. Because CHAMP orbit coverages of the southern polar cap were not extensive, TOI or plasma entry signatures from the dayside cusp to the polar cap were unclear.

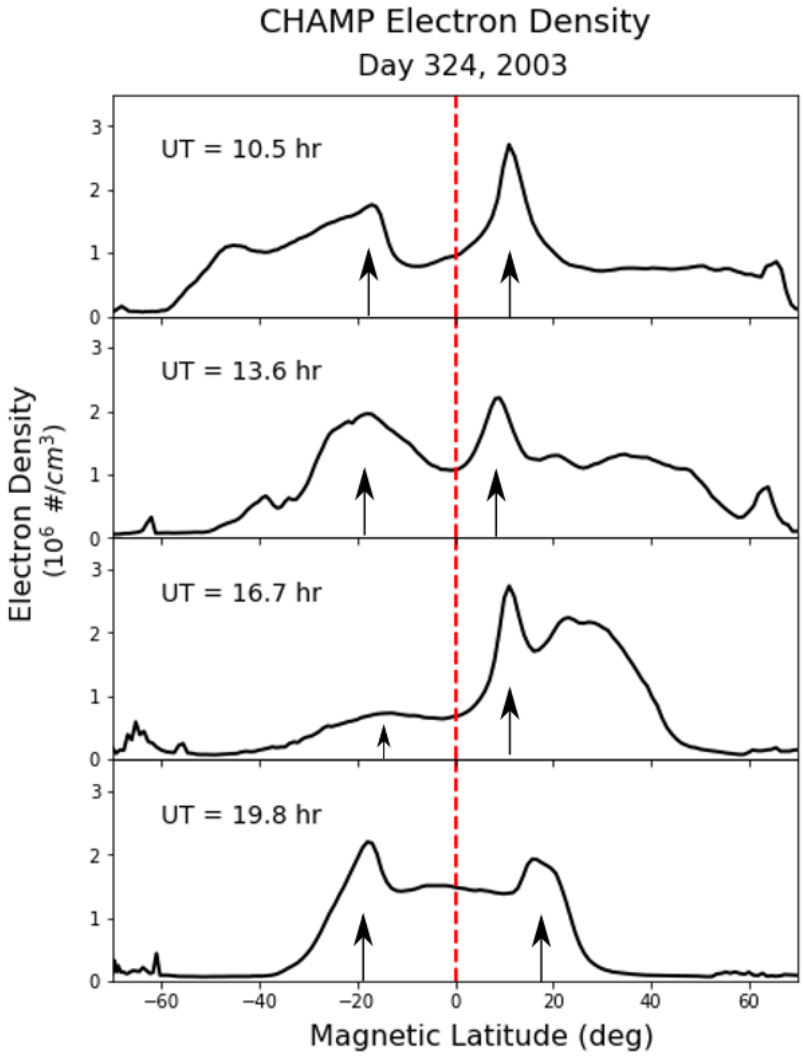

Figure 4. Geomagnetic latitudinal profiles of the in-situ plasma density measured by the CHAMP during four passes. The times when CHAMP crossed the geomagnetic equator are shown in the panels. The red dashed line marks the geomagnetic equator. The arrows point at the magnetic latitudes of the equatorial ionization anomalies.

3.3 Magnetic latitudinal profiles

We produce the electron density magnetic latitudinal profiles for four CHAMP passes (Figure 4), which show distinct density peaks at low latitudes (< 20^o), recognized as the EIA. Along the pass that crossed the equator at 10.5 *hr* UT, the NH SED could be seen as a density

253 enhancement from the EIA to high Mlat (70^o) (top panel). Along the 13.6 *hr* UT orbit, the SED
254 enhancement appeared to withdraw from high magnetic latitudes such that the SED density
255 extension reached only about 50^o Mlat (second panel). The SED retreat was more apparent later
256 at 16.7 *hr* UT (the third panel), with the enhancement extending only to about 40^o even though at
257 a higher level. Later along the 19.8 *hr* UT orbit, CHAMP detected an EIA density enhancement
258 at around 20^o Mlat with a weak density extension into mid-latitudes (bottom panel). In the
259 subsequent passes, CHAMP observed the EIA occurring near the magnetic equator until the end
260 of the day (Figure 2).

261 The observed magnetic latitudinal profiles also display a hemisphere asymmetry. The
262 NH density enhancement was persistently more noticeable than the SH enhancement (Figure 4).
263 This hemisphere asymmetric features may be related to the fact that the SH was in the summer
264 season. The physical reason for the SED hemispheric asymmetry is outside the scope of this
265 paper.
266

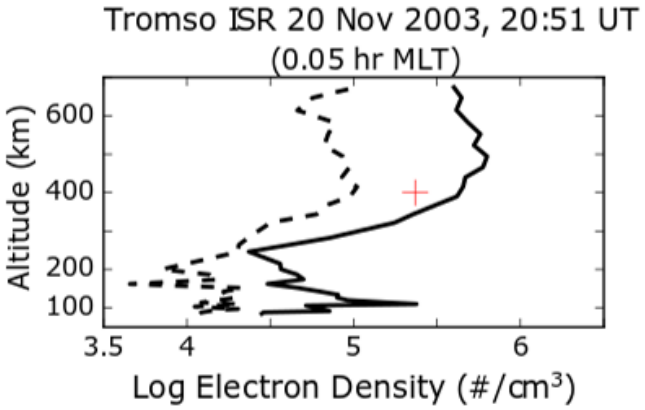

267

268 **Figure 5.** Plasma density measurements by the Tromso ground ISR in conjunction with
269 CHAMP electron density measurements at 390 *km* on 20 November 2003. The Tromso ISR
270 took measurements with an elevation angle of 77.1^o, a mean azimuthal angle of -176^o, and a
271 range from 78 to 678 *km*. The solid line represents electron density measured inside the TOI,
272 whereas the dashed line the background density. The electron density measured by CHAMP in
273 conjunction is plotted as a red + symbol.
274

275 3.4 ISR conjunction observations

276 Foster et al. (2005) reported that the polar TOIs were detected at high latitudes near
277 evening to midnight during the 20 November 2003 magnetic storm recovery phase. A sequence
278 of ISR remote sensings indicated that the TOI was observed at Millstone Hill from 17 to 18 *hr*
279 UT, at Sondrestrom from 18 to 19 *hr* UT, and at EISCAT after 19 *hr* UT. These TOIs had
280 electron density enhancements from 300 to 800 *km*. Here we describe the ground ISR
281 measurements at the EISCAT Tromso station in conjunction with the CHAMP observations.

282 The EISCAT UHF system at Tromso station was operated with a 32 *m* antenna at a
283 frequency range around 929 *Mhz* at a geographic location of 69◦350 N latitude and 19◦140 E

longitude. We downloaded its ISR data file NCAR_2003-11-20_tau2pl_uhf.bin.hdf5 from the CEDAR Madrigal website (http://cedar.openmadrigal.org/). According to its metadata file, the Tromso UHF system took measurements with an elevation angle of 77.1^{o}, a mean azimuth of -176^{o,} and a range from 78 to 678 *km*.

For several passes over Tromso, CHAMP encountered plasma clouds in conjunction with EISCAT Tromso ISR measurements. For example, the ISR observed density enhancement from 200 to 800 *km* at 20:51 UT (solid line, Figure 5). The peak logarithmic density at about 500 *km* was $log_{10}Ne$ ~ 5.8, about 1.5 times enhancement from the background density (dashed line) before the TOI was detected. The plasma cloud logarithmic density measured by CHAMP at 390 *km* was about $log_{10}Ne$ = 5.4, close to that measured by the Tromso ISR at that altitude (marked by a red + symbol).

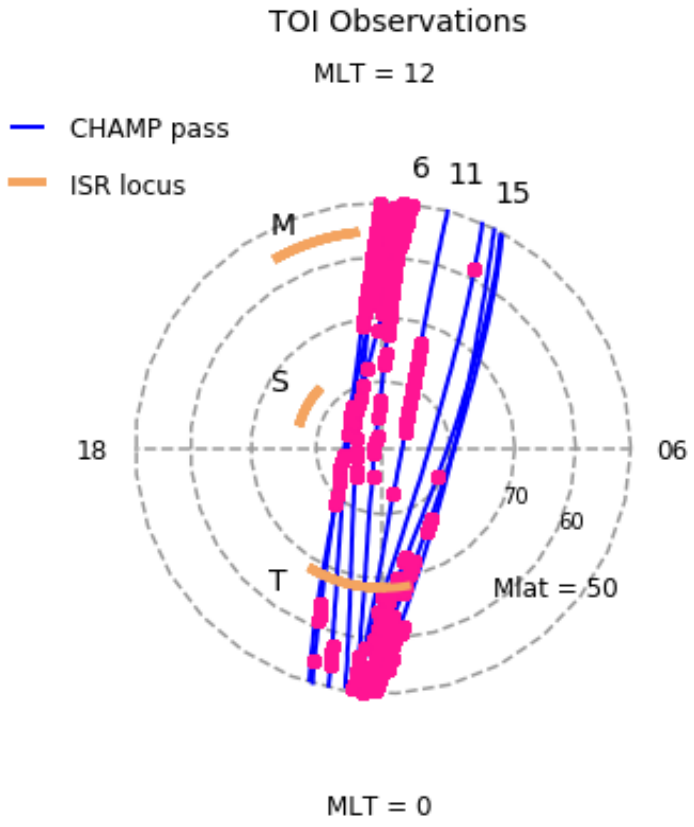

Figure 6. Locations of plasma clouds detected by CHAMP in the polar cap on 20 November 2003, from 08:00 UT to the end of the day. Each filled pink circle represents a location where the CHAMP logarithmic density measurement $log_{10}Ne$ was greater than 5.5. The number of the orbit passes during the day was displayed at the top of the 50^{o} Mlat circle. CHAMP detected the plasma clouds from the 6th pass to the 15th pass of the day. The loci of ISR stations in the interval of TOI detection are presented as amber color curves. M marks the ISR locus for the Milton Hill station, S for the Sonderstrom station, and T for the Tromso station.

Figure 6 presents locations of plasma clouds detected by CHAMP in the polar cap with $log_{10}Ne$ greater than 5.5 from 08:00 UT to the end of the day (shown as filled pink circles).

CHAMP detected these plasma clouds during nine orbit passes starting on the 6th pass of the day from 08:00 to 24:00 UT. The detected polar plasma clouds were distributed uniformly from noon to midnight MLT during the first five passes (6th – 11th pass). During the later passes (12th – 15th pass), CHAMP encountered plasma clouds around midnight MLT near the auroral zone magnetic latitudes (50^{o} – 70^{o} Mlat). Figure 6 also shows the loci of the ISR stations on the polar cap plot when detecting TOIs (amber color curves). The Milton Hill station observed the TOI at 55^{o} Mlat during late afternoon MLT (marked by M). The Sondrestrom station was at ~78^{o} Mlat around 17 MLT (marked by S), and the Tromso at ~68^{o} Mlat from 22 – 01 MLT (marked by T). Milton Hill ISR detected TOI during the 12th CHAMP orbit pass, Sondrestrom during the 13th pass, and Tromso during both the 14th and 15th orbit passes. Thus, CHAMP intersected polar cap plasma clouds throughout the whole duration of the magnetic storm. At the same time, these ISR stations remotely sensed the TOIs only during the storm recovery phase due to the absence of daytime observation. Another distinct difference is that CHAMP detected the polar plasma clouds near the noon-midnight plane from 70^{o} Mlat near noon to 50^{o} Mlat near midnight, whereas the ISR stations detected the polar cap patches or TOIs on the dusk side and near the midnight polar cap.

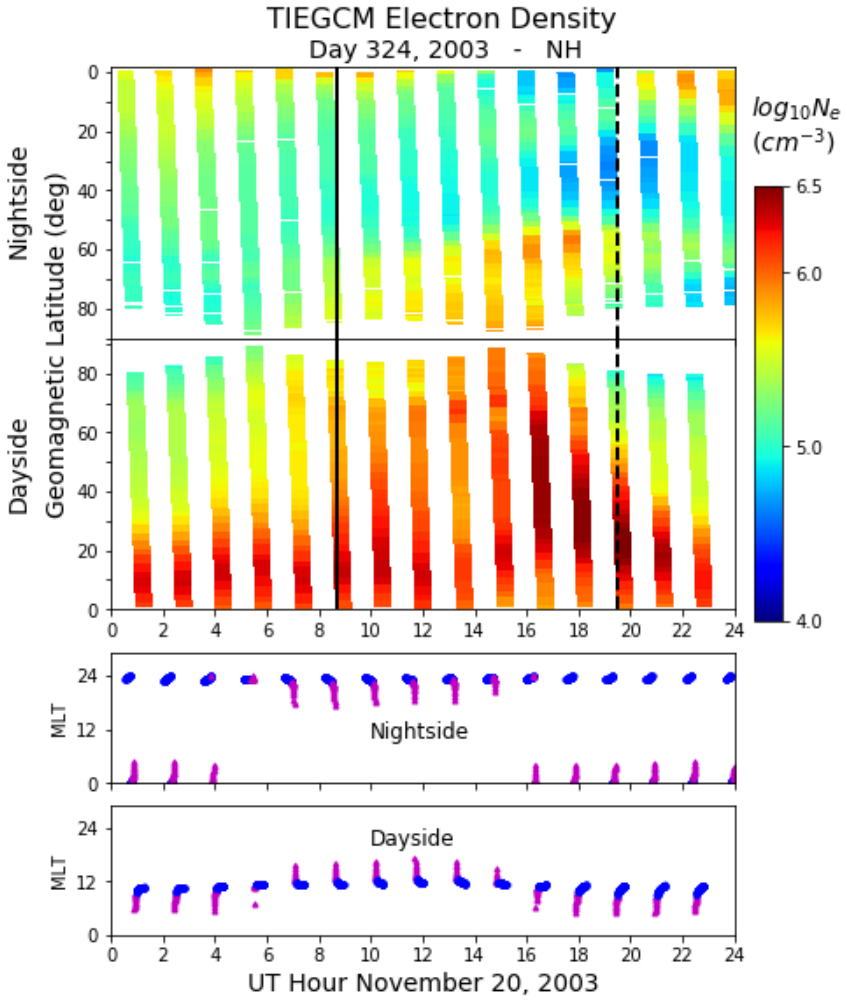

Figure 7. Plasma density along the CHAMP satellite orbit in the NH on 20 November 2003 modeled by TIEGCM presented in the same format as Figure 2.

4 TIEGCM Modeling

We conducted TIEGCM modeling for the 20 November 2003 magnetic storm to understand the SED and TOI lifecycle. We used the TIEGCM version 2.0 with a 2.5-degree resolution in latitude and longitude and a time step of 30 seconds. The default potential model, the Heelis Model, was used. The TIEGCM source file used for this run is the same as the benchmark run available on the TGCM website (http://www.hao.ucar.edu/). Overall, the TIEGCM modeling for this day shows appreciable plasma density enhancements at noon in both hemispheres and the polar cap after the storm onset (see the demo results http://www.hao.ucar.edu/). To compare the TIEGCM modeling results with the CHAMP observations, we plot the modeled plasma density along the CHAMP satellite orbit in geomagnetic coordinates and display the modeled plasma density for the NH and SH in Figures 7 and 8, respectively. Because the TIEGCM model generates diagnosis variables in the geographic coordinates, we interpolate these variables at the CHAMP geomagnetic coordinates to facilitate comparison.

Figure 7 shows that TIEGCM's NH electron density variation is similar to CHAMP observations, although the details differ. It shows the SED electron density enhancement onset at 07 *hr* UT, about one orbit earlier than CHAMP detection (marked by the black line in Figure 7). The modeling indicates mid-latitude electron density enhancement extending to high latitudes (~65^o Mlat) from 08 till 18 *hr* UT. In contrast, CHAMP revealed a shorter duration of mid-latitude electron density enhancement extension to the cusp from 09 to 15 *hr* UT. A clear electron density boundary is evident on the nightside starting at about 70^o Mlat at the beginning of the SED event (~ 10 *hr* UT) and lowering to a low Mlat of 60^o at 18 *hr* UT (Figure 7, top panel). This nightside boundary feature is similar to that detected at 50^o Mlat by CHAMP from 10 to 24 *hr* UT (Figure 2, top panel). This nightside electron density boundary might be related to the occurrence of the nighttime mid-latitude ionospheric trough associated with subauroral polarization streams (SAPS) during magnetic storms (Wang et al., 2008; He et al., 2011).

The TIEGCM modeling displays retreat features of the SED electron density enhancement significantly different from the CHAMP observations. The modeled NH electron density begins to withdraw from high to low Mlat after 20 *hr* UT when *Sym-H* starts to recover (marked by the dashed line in Figure 7), whereas the observed SED retreat started about 15 *hr* UT. At that time, the magnetic storm was still in the main phase. We suspect that the Heelis polar cap potential model used in the modeling has not sufficiently accounted for actual variations of the cross-polar cap potential and resulted in a delay in the SED retreat.

There are other minor differences between the TIEGCM modeling and CHAMP observations. For example, the TIEGCM modeling shows a more vigorous SED onset than the CHAMP observations (see Figures 2 and 7). In addition, the modeled NH electron density is enhanced up to 90^o MLat, while the detected enhancement is evident only up to about 65^o MLat. In addition, TIEGCM modeling indicates a smooth entry of plasma through the dayside cusp into the polar cap, whereas CHAMP detected more patch structures. We attribute these minor differences to modeling grid resolution and other limitations.

The SH modeling generally exhibits mid-latitude electron density enhancement after 10 *hr* UT (Figure 8). Notably, there are several disagreements with the CHAMP observations shown in Figure 3. For example, the TIEGCM modeled density presented in the second panel of Figure 8 is void of an SH precursory density enhancement. In contrast, CHAMP observed the precursor before 08 *hr* UT (Figure 3, second panel). Furthermore, TIEGCM's SH modeling has not produced features of density retreat to lower MLat as exhibited in the CHAMP SH spectrogram after 09 *hr* UT (Figure 3, second panel). The causes of these disagreements are unclear.

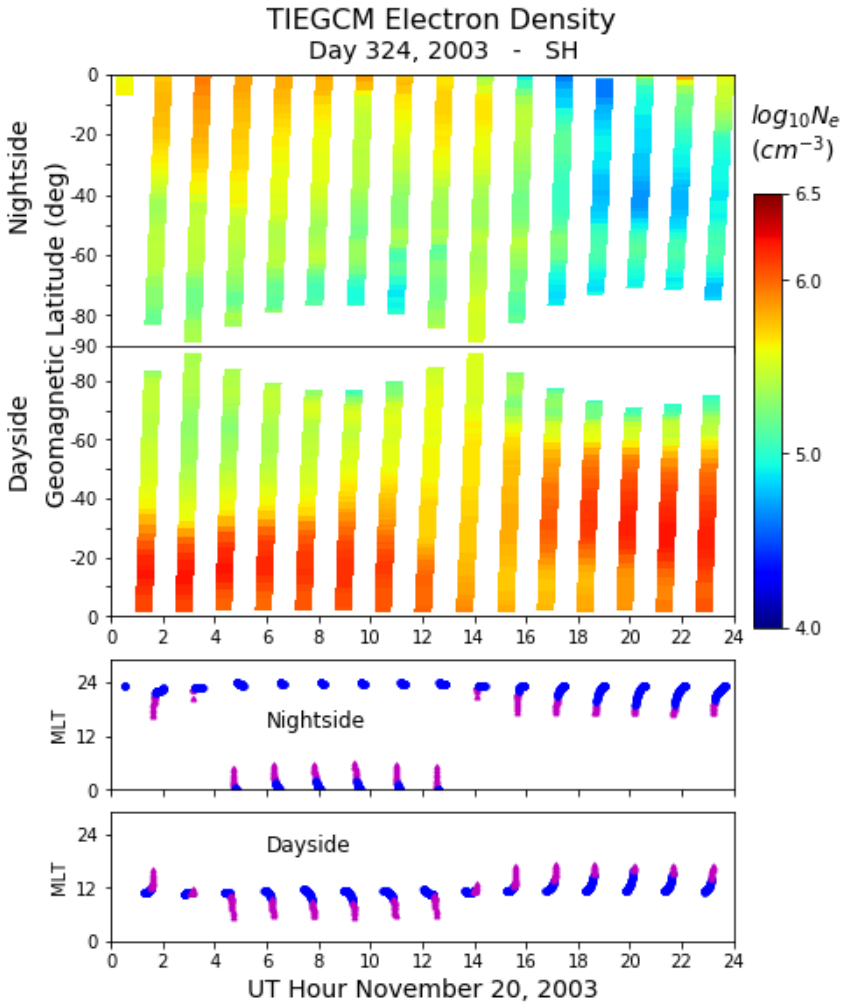

Figure 8. Plasma density along the CHAMP satellite orbit in the SH on 20 November 2003 modeled by TIEGCM presented in the same format as Figure 3.

5 Discussions

This paper analyzed in-situ electron density observations of the SED and its associated polar cap TOI/plasma clouds in the F region near the noon meridian plane by the CHAMP

satellite during the 20 November 2003 storm. The CHAMP satellite in-situ measurements reveal new distinct characteristics about the SED. Moreover, the long duration of observing the SED on a given meridional plane throughout the whole period of the magnetic storm sheds light on its life cycle that is unclear before. The new results are summarized below.

1. Mid-latitude SED electron density in the NH was enhanced right after the ICME shock front arrival and before the magnetic storm main phase developed in earnest.
2. The SED electron density enhancement extended from the EIA to the noon cusp, through which plasmas entered into the polar cap as polar plasma clouds/TOI.
3. The SED plume near the noon meridian plane in the NH retreated gradually to lower latitudes six hours after the SED onset. In contrast, SH mid-latitude electron density enhancement in the same plane withdrew toward the equator soon after the NH SED buildup.
4. The CHAMP and EISCAT ISR simultaneous conjunction observations provide the first direct evidence that polar cap plasma patches/clouds with a density greater than 10^5 #/cm^3 at about 390 *km* were the polar TOI measured remotely by the ground stations.

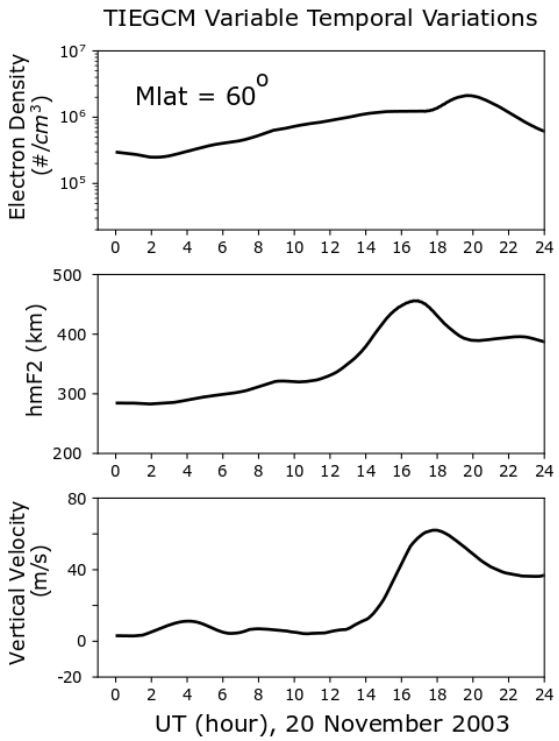

Figure 9. Plasma density, hmF2 height, and ion vertical *E*x*B* drift velocity at Mlat = 60° in the NH on 20 November 2003 modeled by TIEGCM. The panels display the modeled plasma density, the hmF2 height, and the ion vertical velocity from top to bottom.

We have compared TIEGCM modeling with the CHAMP observations to learn SED's physical processes. The temporal variations of mid-latitude electron density at noon MLT in the NH from the TIEGCM modeling generally agree with CHAMP's SED observations, even though the modeled timeline tends to be off (see Figures 2 and 7). Figure 9 further illustrates temporal variations of several variables at Mlat = 60^o in the NH. The modeled electron density at Mlat = 60^o increases steadily starting from the ICME shock arrival at 8 *hr* UT (top panel) in agreement with the observed density. However, it pulls back from a peak density after 20 *hr* UT, later than the retreat observed around 15 *hr* UT. The hmF2 height has a similar temporal variation (Figure 9, middle panel). It increases from 300 *km* at the beginning of the storm to over 450 *km* at the peak of magnetic disturbance (18 *hr* UT). Associated with the hmF_2 height increase, ion vertical *E*x*B* drift velocity component W_{ExB} increases appreciably to as high as 60 *m/s* during the magnetic storm (Figure 9, bottom panel). This W_{ExB} increase would raise the hmF_2 height and account for the density enhancement. This interpretation agrees with J. Liu et al. (2016). They deployed TIEGCM to identify the principal mechanisms for the SED and TOI through a term-by-term analysis of the ion continuity equation. Their study showed that upward *E*x*B* ion drifts in the topside ionosphere are most important in the SED formation. The drift effects are offset by antisunward neutral winds and downward ambipolar diffusion effects. They thus concluded that the SED signature in TEC is mainly caused by upward *E*x*B* ion drifts that lift the ionosphere to higher altitudes where chemical recombination is slower.

Foster et al. (2005) have examined ISR measurements for this storm event and concluded that the SED and its associated TOI occurred in later afternoon and evening sectors during the recovery phase. Mannucci et al. (2008) studied the mid-latitude vertical TEC for altitudes above the satellite measured by the CHAMP satellite for this event too. They performed a superposed epoch analysis of the TEC response by defining the start time of the epoch when the interplanetary electric field (IEF) computed first reaches ten *mV/m* during a period of continuously southward B_z. Using the formula by Kan and Lee (1979), they calculated the IEF as $E_{sw} = |V_x|B_T \sin^2(\psi/2)$, where V_x is the eastward velocity in the GSM coordinate, B_T is the component perpendicular to the Earth-Sun line, and ψ is the rotation angle of the interplanetary plane in the y-z plane. The significant TEC increase appeared 5-7 hours following the defined IEF epoch start time (11:22 UT), while the rest of the storm events had an ionospheric response within 1-2 *hr* of the specified start time. They regarded the long delay in TEC increase after the IEF epoch start time during the 20 November 2003 event as unusual. They attributed the unusual TEC storm behavior to relatively mild *Bz* southward conditions before the storm onset. Interestingly, the present study indicates that the in-situ electron density at about 390 *km* increased immediately after the ICME shock arrival. According to Yizengaw et al. (2006), the dayside F2-layer peak height from the ground ionosonde profiles was initially below 350 *km* during this event. These satellite and ground ionosonde observations together imply that the electron density above 400 *km* did not substantially increase until the later phase of the magnetic storm (>~ 18 *hr* UT). This conclusion is also consistent with the temporal variation of hmF_2 from the TIEGCM modeling shown in Figure 9.

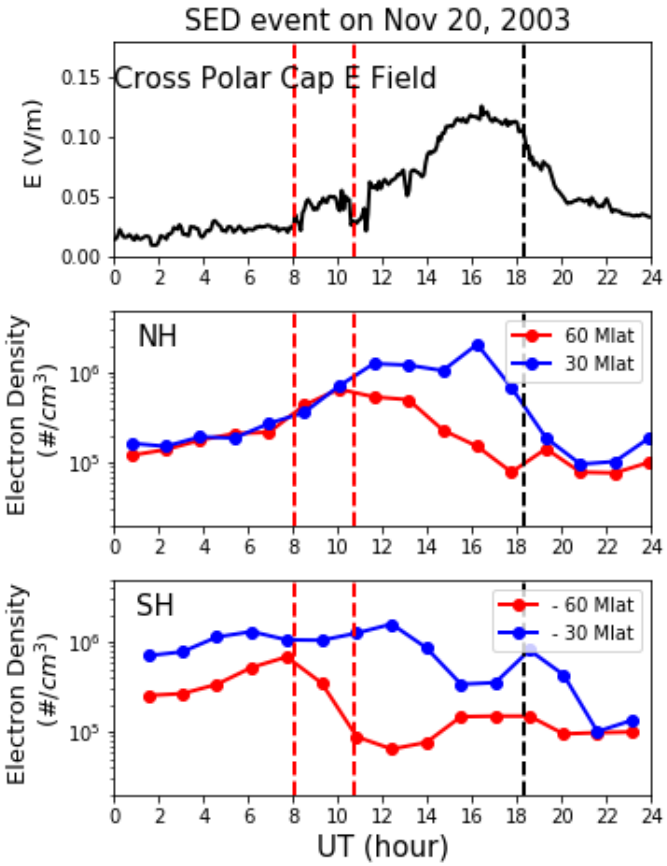

Figure 10. Cross-polar cap electric field E_{PC} (top panel) together with NH plasma densities (middle panel) and SH plasma densities (bottom panel) during 20 November 2003. The NH plasma density at 30^o (blue line, middle panel) varies closely with E_{PC}. The NH plasma density at 60^o (red line, middle panel) indicates an approximately similar variation with E_{PC}. The SH plasma densities at 30^o and 60^o (blue and red lines in the bottom panel, respectively) have not displayed a similar variation with E_{PC}.

5.1 Prompt penetration electric fields

The convective electric fields responsible for the upward ion drifts and rising hmF2 height are probably primarily contributed by the prompt penetration electric fields (PPEFs). The IEF produces the cross-polar cap electric field (EPC) from dawn to dusk across the polar cap during magnetic storms. A fraction of E_{PC} can penetrate to mid and low latitudes via current leakage through the conducting ionosphere, yielding an eastward zonal electric field on the dayside and a westward electric field on the nightside (Fejer and Scherliess, 1995, 1997). The PPEFs typically respond in minutes to variations in the IEF, and the penetration efficiency is highest near local noon compared to other local times (Manoj et al., 2008). Retterer and Kelley (2010) conducted equatorial ionosphere modeling to understand variations of the plasma densities measured by the Jicamarca ISR and the total electron content (TEC) measured by the Boston College South American chain of GPS receivers. They found that 10% penetration of the IEF to the equator is sufficient for the modeling to achieve good agreement. Manucci et al.

(2014) studied ionospheric response for different superstorms. They suggested that the PPEF produced by the leakage of the cross-polar cap potential and Region 1 currents is a significant factor affecting TEC variations. They asserted that magnetospheric shielding currents have developed and/or the thermospheric dynamics have evolved during the geomagnetic disturbance, causing the TEC to decrease from its peak storm-time value.

The IEF effects on mid-latitude TEC response had been examined by Mannucci et al. (2008) using E_{SW}. Here we look into the IEF effects using E_{PC} on electron density at mid-latitudes. We define E_{PC} as Φ_{PC}/L_x, where Φ_{PC} is the cross-polar cap dawn-to-dusk potential and L_x is the open-closed boundary (OCB) length in the dawn-dusk direction. We employ the Boyle empirical model to estimate Φ_{PC} as

$$\Phi_{PC} = 1.01\text{x}10^{-4} V_T^2 + 11.7\,|B|\sin^3(\theta/2) \qquad (6)$$

where V_T is the solar wind speed in *km/s*, B is the magnitude of the IMF in nanotesla and $\theta = \cos^{-1}(B_Z/B)$ (Boyle et al., 1997). We have determined L_x and the OCB by tracing field lines from the 400 *km* topside ionosphere to the magnetosphere using the double-precision GEOPACK-2008_dp package (Lin et al., 2018). We traced magnetic field lines using two data-based magnetic field models: the TS05 model (Tsyganenko and Sitnov, 2005) for the inner magnetosphere and the Tsyganenko T96 model (Tsyganenko, 1995) for the outer magnetosphere. It is advantageous to use E_{PC} over E_{SW} as a PPEF proxy because E_{PC} is closer than E_{SW} relative to PPEF. Furthermore, E_{SW} could not infer PPEFs for northward B_z because E_{SW} becomes negative. As a result, the PPEF is set to zero for $B_z > 0$. In contrast, E_{PC} for $B_z > 0$ would merely reduce the dawn-to-dusk PPEF's magnitude.

Figure 10 from top to bottom presents E_{PC} (top panel), NH plasma densities at 30^o and 60^o Mlat, respectively (middle panel), and SH plasma densities at -30^o and -60^o Mlat (bottom panel), respectively. The NH electron density (blue line, middle panel) closely follows E_{PC} variation at 30^o through the whole storm interval. In contrast, the NH electron density at 60^o and E_{PC} behave similarly only for a few hours (10 -12 *hr* UT) after the SED onset (red line, middle panel). Noticeably, the SH plasma densities at 30^o and 60^o have not displayed a similar variation with E_{PC} (blue and red lines in the bottom panel, respectively). We perform a regression analysis of NH electron density at 30^o versus E_{PC}. The NH electron density at 30^o is linearly correlated with E_{PC} with the R^2 coefficient of determination of 0.8 for a time interval from 0 to16 *hr* UT (Figure 11). However, the R^2 coefficient of determination decreases to 0.5 when the time interval is extended to 22 *hr* UT even though the NH electron density at 30^o followed the E_{PC} decrease. This apparent correlation indicates a likely extension of E_{PC} to mid-latitudes that results in density enhancements. We thus assert that the NH mid-latitude electron density varies in response to PPEF variations produced by E_{PC}. This conclusion is consistent with the previous interpretations about the storm-time mid-latitude TEC variations by Mannucci et al. (2008) and Mannucci et al. (2014).

We interpret the lack of correlation between E_{PC} and the SH electron density due to the effective shielding of PPEF in the SH. In contrast to NH observations, SH mid-latitude electron density enhancement retreated to lower latitudes soon after the NH SED buildup. Since the SH was in the summer season, larger SH ionospheric plasma densities may have shielded E_{PC} at mid-latitudes. In addition, the negative storm effects due to changes in thermospheric composition or O/N2 depletion may cause the asymmetric hemisphere response to E_{PC} (Burns et al., 2007). Future studies are needed to apprehend this hemisphere asymmetry.

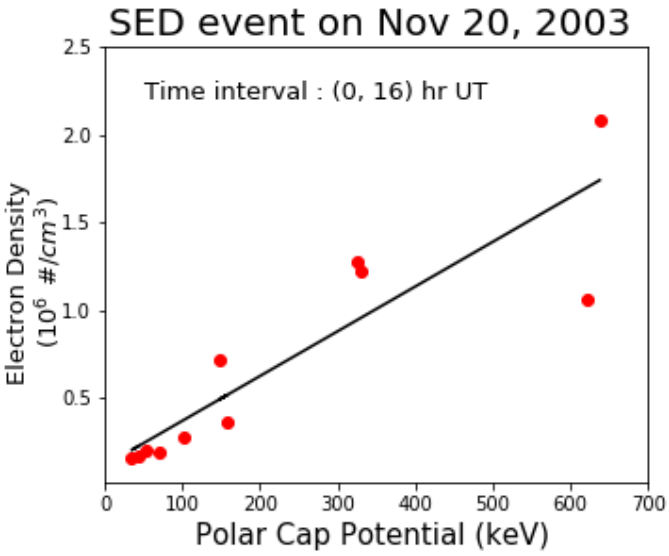

Figure 11. Linear correlation of NH plasma densities at 30^o with E_{PC} for a time interval from 0 to 16 *hr* UT.

5.2 SED life cycle

The SED life cycle observed by the CHAMP satellite likely reflects the dayside PPEF temporal variation. After the SED onset, CHAMP observed the in-situ electron density from low latitudes to 60^o Mlat for about 3 hours (see Figure 2). This feature suggests that an absence of electric fields may have allowed the PPEF to extend to the cusp. It is plausible that ring current had not evolved to shield the dayside PPEF immediately after the ICME shock arrival as magnetosphere magnetic fields stretched to the tail side. However, as the ring current moves closer to the dayside Earth, shielding reduces mid-latitude electric fields. After about 14 *hr* UT, the electron density at 60^o Mlat started to decay. From 15 to 20 *hr* UT, the SED gradually retreated toward the EIA peak magnetic latitude (20^o) (Figure 2), probably responding to PPEF variation due to the extension of shielding toward lower magnetic latitudes. The eventual disappearance of the EIA after 20 *hr* UT would imply an absence of the PPEF.

This interpretation does not rule out other additional factors contributing to the SED retreat. For example, disturbance dynamo electric fields generated by storm time winds could have weakened the PEFF *(*Fejer and Scherliess, 1995*)* and contributed to the SED retreat. Besides zonal electric field variations, other factors influencing the SED decay include an increase in the plasma loss rate and an expansion of equatorward meridional wind (J. Liu et al., 2016). In addition, the SED retreat might have resulted from a depletion of electron density when recombination with neutrals is enhanced. In this scenario, the SED retreat would imply equatorward motion of high-density neutral gas. It is also possible that the SED moved outside of the noon meridional plane as it is very dynamic. Future analyses of PPEF and neutral density observations at mid-latitudes would help clarify the mechanisms causing the SED decay.

Multiple CHAMP passes over the polar cap also shed light on TOI's life cycle. A TOI is generally believed to be originated from the dayside mid-latitudes during the recovery phase (Foster et al., 2005). The CHAMP observations reported here indicate that a TOI entered the polar cap through the noon sector during the magnetic storm main phase. The CHAMP satellite did not observe the TOI plasma clouds at latitudes lower than the nightside auroral boundary, suggesting that the TOI plasma clouds drift westward azimuthally toward the dusk sector under intense auroral zone electric fields. Since ISR observations have indicated that the TOI had entered into the polar cap from the dusk sector during the recovery phase (Foster et al., 2005), they might have re-entered into the polar cusp from the dusk side and appeared again as TOI circulating in the polar cap.

We have previously studied polar cap plasma clouds associated with TOIs during magnetic storm events (Lin et al., 2018). These plasma clouds had a density greater than $1x10^5$ $\#/cm^3$ and scale size of less than 1000 *km*. In addition, they were simultaneously detected near polar-cap neutral density enhancement regions by a factor 10 above the background value. We have thus suggested that these TOI plasma clouds play an important role in producing thermospheric density anomalies through enhanced ion-neutral collisions.

6 Conclusions

We report for the first time satellite in-situ observations of a dayside mid-latitude SED and its associated polar TOI at the noon meridional plane during the 20 November 2003 storm triggered by an ICME shock passing through Earth. The CHAMP satellite observations render rare documentation about the SED's life cycle at a fixed magnetic local time through multiple passes, demonstrating its onset, retreat, and entry into the polar cap as TOI. We show that the mid-latitude electron density varied with the cross-polar cap electric fields, indicating that prompt penetration electric fields in the zonal direction played a dominant role in producing the SED. We thus suggest that the SED lifecycle is mainly controlled by variations of the dayside penetrating electric fields. The TIEGCM modeling further explains that enhancement of the zonal electric fields transports plasmas higher, leading to mid-latitude density enhancement. The observed SED was more pronounced in the NH hemisphere than the SH hemisphere, displaying asymmetrical ionospheric responses to the ICME shock passage. However, the SED hemisphere asymmetrical features remain unexplained. More observations and global circulation modeling are needed to understand better the physical processes of generating the SED due to magnetosphere-ionosphere-thermosphere interactions.

Acknowledgments and Data

The CHAMP plasma density dataset is available from ftp://isdcftp.gfz-potsdam.de/champ/ME/Level3/. We thank Ingemar Häggström, EISCAT Scientific Association, for permission to use EISCAT data for this study. The Tromso ISR data file is retrieved from the CEDAR Madrigal database. National Center for Atmospheric Research is sponsored by the National Science Foundation.

References

Adebiyi, S. J., Ikubannia, S. O., Adebesina, B. O., Joshuab, B. W., & Adekoyac, B. J. (2019), Variations of GPS-TEC at an African Low Latitude Station during Geomagnetic Disturbances, *Phys. Memoir* 1, 113–125, http://jtap.physicsmoir.com.ng

Anderson, D. N. (1976). Modeling the midlatitude F-region ionospheric storm using east-west drift and a meridional wind, *Planet. Space Sci.,* 24, 69–77, doi:10.1016/0032-0633(76)90063-5

Boyle, C. B., Reiff, P. H., & Hairston, M. R. (1997). Empirical polar cap potential, *J. Geophys. Res.,* 102, 111-125.

Buonsanto, M. J. (1995). Millstone Hill incoherent scatter F region observations during the disturbances of June 1991, *J. Geophys. Res.,* 100, 5743–5755, doi:10.1029/94JA03316.

Buonsanto, M. J. (1999). Ionospheric storms: A review, *Space Sci. Rev.,* 88, 563–601, doi:10.1023/A:1005107532631

Burns, A. G., Solomon, S. C., Wang, W., & Killen, T. L. (2007). The ionospheric and thermospheric response to CMEs: Challenges and success, *J. Atmos. Solar-Terrs. Phys*., 69, 77-85.

Cooke, D. L., Turnbull, W., Roth, C., Morgan, A., & Redus, R. (2003). Ion drift-meter status and calibration, in *First Champ Mission Results for Gravity, Magnetic, and Atmospheric Studies,* edited by Reigber, C., Luhr, H., and Schwintzer, P., Springer, New York, pp. 212–219.

Correia, E., Spogli, L., Alfonsi, L., Cesaroni, C., Gulisano, A. M., , Thomas, E. G., et al. (2017), Ionospheric F-region response to the 26 September 2011 geomagnetic storm in the Antarctica American and Australian sectors, *Ann. Geophys.,* 35, 1113–1129, https://doi.org/10.5194/angeo-35-1113-2017

Coster, A., & Skone, S. (2009). Monitoring storm-enhanced density using IGS reference station data, *J. Geod.* (2009) 83:345–351, DOI 10.1007/s00190-008-0272-3

Crowley, G., Knipp, D. J., Drake, K. A., Lei, J., Sutton, E., & Luhr, H. (2010). Thermospheric density enhancements in the dayside cusp region during strong B_Y conditions. *Geophys. Res. Lett.*, 37, L07110. https://doi.org/10.1029/2009GL042143

Echer, E., Gonzalez, W. D., & Tsurutani, B. T. (2008). Interplanetary conditions leading to superintense geomagnetic storms (Dst ≤ – 250 nT) during solar cycle 23, *Geophys. Res. Lett.,* 35, L06S03, doi:10.1029/2007GL031755

Evans, J. V. (1973). The causes of storm-time increases of the F-layer at midlatitudes, *J. Atmos. Terr. Phys.,* 35, 593–616, doi:10.1016/0021-9169 (73)90191-8

Fejer, B.G., & Scherliess, L., 1995. Time dependent response of equatorial ionospheric electric fields to magnetospheric disturbances. *Geophys. Res. Lett.* 22, 851–854.

Fejer, B.G., & Scherliess, L., 1997. Empirical models of storm time equatorial zonal electric fields. *J. Geophys. Res.* 102, 24,047.

Foster, J. C. (1993). Storm-time plasma transport at middle and high latitudes, *J. Geophys. Res.,* 98, 1675–1689, doi:10.1029/92JA02032

Foster, J. C., Coster, A. J., Erickson, P. J., Holt, J. M., Lind, F. D., Eideout, W., et al. (2005). Multiradar observations of the polar tongue of ionization, *J. Geophys. Res.*, 110, A09S31, doi:10.1029/2004JA010928

Han, J, P., Wang, C., & Li H. (2014). Energetics characteristics of the super magnetic storm on 20 November 2003 based on 3D global MHD simulation. *Science China: Earth Sciences*, doi: 10.1007/s11430-014-5013-2

He, M., Liu, L., Wan, W. & Zhao B. (2011), A study on the nighttime midlatitude ionospheric trough, *J. Geophys. Res.*, 116, A05315, doi:10.1029/2010JA016252

Horvath, I., & Lovell, B. C. (2015), Storm-enhanced plasma density and polar tongue of ionization development during the 15 May 2005 superstorm, *J. Geophys. Res. Space Phys.*, 120, 5101–5116, doi:10.1002/2014JA020980

Kan, J. R., & Lee, L. C. (1979), Energy coupling function and solar wind magnetosphere dynamo, *Geophys. Res. Lett.*, 6, 577– 580, doi:10.1029/GL006i007p00577

Lin, C. S., Sutton, E. K., Huang, C. Y., & Cooke, D. L. (2018). Occurrence locations, dipole tilt angle effects, and plasma cloud drift paths of polar cap neutral density anomalies. *J. Geophys. Res. Space Phys.*, 123. https://doi.org/10.1002/2017JA024657

Liu, H., Stolle, C., Forster, M., & Watanabe, S. (2007), Solar activity dependence of the electron density in the equatorial anomaly regions observed by CHAMP, *J. Geophys. Res.*, 112, A11311, doi:10.1029/2007JA012616

Liu, J., Nakamura, T., Liu, L., Wang, W., Balan, N., Nishiyama, T., et al. (2015). Formation of polar ionospheric tongue of ionization during minor geomagnetic disturbed conditions, *J. Geophys. Res. Space Phys.*, 120, 6860–6873, doi:10.1002/2015JA021393

Liu, J., Wang, W., Burns, A., Solomon, S. C., Zhang, S., Zhang, Y., & Huang, C. (2016). Relative importance of horizontal and vertical transports to the formation of ionospheric storm-enhanced density and polar tongue of ionization, *J. Geophys. Res. Space Phys.*, 121, 8121–8133, doi:10.1002/2016JA022882

Lühr, H., & Xiong, C. (2010), IRI-2007 model overestimates electron density during the 23/24 solar minimum, *Geophys. Res. Lett.*, 37, L23101, doi:10.1029/2010GL045430

Mannucci, A. J., Crowley, G., Tsurutani, B. T., Verkhoglyadova, O. P., Komjathy, A., & Stephens, P. (2014). Interplanetary magnetic field by control of prompt total electron content increases during superstorms. *J. Atmos. Solar-Terr. Phys.*,115–116, 7–16. https://doi.org/10.1016/j.jastp.2014.01.001

Mannucci, A. J., Tsurutani, B. T., Abdu, M. A., Gonzalez, W. D., Komjathy, A., Echer, E., et al (2008). Superposed epoch analysis of the dayside ionospheric response to four intense geomagnetic storms, *J. Geophys. Res.*, *113*, A00A02, doi:10.1029/2007JA012732

Manoj, C., Maus, S., Lu¨hr, H., & Alken, P. (2008), Penetration characteristics of the interplanetary electric field to the daytime equatorial ionosphere, *J. Geophys. Res.*, 113, A12310, doi:10.1029/2008JA013381

McNamara, L. F., Cooke, D. L., Valladares, C. E., & Reinisch, B. W. (2007). Comparison of CHAMP and Digisonde plasma frequencies at Jicamarca, Peru, *Radio Sci.*, 42, RS2005, doi:10.1029/2006RS003491

Mendillo, M., Papagiannis, M. D., & Klobuchar, J. A. (1972). Average behavior of the midlatitude F-region parameters NT, Nmax and τ during geomagnetic storms, *J. Geophys. Res.*, 77, 4891–4895, doi:10.1029/JA077i025p04891

Papagiannis, M. D., Mendillo, M., & Klobuchar, J. A. (1971). Simultaneous storm-time increases of the ionospheric total electron content and the geomagnetic field in the dusk sector, *Planet. Space Sci.*, 19, 503–511, doi:10.1016/0032-0633(71)90166-8

Retterer, J. M., & Kelley, M/ C. (2010), Solar wind drivers for low-latitude ionosphere models during geomagnetic storms, *J. Atmos. Solar-Terr. Phys.*, 72, 344–349, doi:10.1016/j.jastp.2009.07.003

Sori, T., Shinbori, A., Otsuka, Y., Tsugawa, T., & Nishioka, M. (2019). Characteristics of GNSS total electron content enhancements over the midlatitudes during a geomagnetic storm on 7 and 8 November 2004. *J. Geophys. Res. Space Phys.*, 124, https://doi.org/10.1029/2019JA026713

Tsyganenko, N. A. (1995), Modeling the Earth's magnetospheric magnetic field confined within a realistic magnetopause. *J. Geophys. Res.*, 100, A4, 5599-5612.

Tsyganenko, N. A., & Sitnov, M. I. (2005), Modeling the dynamics of the inner magnetosphere during strong geomagnetic storms, *J. Geophys. Res.*, 110, A03208, doi:10.1029/2004JA010798

Verkhoglyadova, O. P., Komjathy, A., Mannucci, A. J., Mlynczak, M. G., Hunt, L. A., & Paxton, L. J. (2017). Revisiting ionosphere-thermosphere responses to solar wind driving in superstorms of November 2003 and 2004. *J. Geophys. Res. Space Phys.*, 122, 10,824–10,850. https://doi.org/10.1002/2017JA024542

Wang, H., Ridley, A. J., Lu¨hr, H., Liemohn, M. W., & Ma, S. Y. (2008). Statistical study of the subauroral polarization stream: Its dependence on the cross-polar cap potential and subauroral conductance, *J. Geophys. Res.*, 113, A12311, doi:10.1029/2008JA013529

Yizengaw, E., Moldwin, M. B., Komjathy, A., & Mannucci, A. J. (2006). Unusual topside ionospheric density response to the November 2003 superstorm, *J. Geophys. Res.*, 111, A02308, doi:10.1029/2005JA011433

Yue, X., Wan, W., Liu, L., Liu, J., Zhang, S., Schreiner, W. S., et al. (2016), Mapping the conjugate and corotating storm-enhanced density during 17 March 2013 storm through data assimilation, *J. Geophys. Res. Space Physics*, 121, 12,202–12,210, doi:10.1002/2016JA023038